Technical Report

UDC 669 . 15 ' 24 : 548 . 4

In situ Dislocation Substructure Analysis of Fe-30 mass% Ni Martensitic Alloy

Mitsuharu YONEMURA* Tomohiro NISHIURA

Abstract

In order to observe the recovery and the phase transformation of the Fe-30 mass%Ni lenticular martensitic alloy quantitatively, X-ray line profile analysis in consideration of elastic anisotropy was applied to the high temperature X-ray diffraction pattern of the sub-zero treated alloy, and observed the behavior of the dislocation density and character at the elevated temperature. It was collaborated with an observation of the dislocation substructure by TEM observation, the ECCI and the local lattice strain by EBSD pattern. Consequently, the dislocation density is inherited in the reverse transformation from α' phase to γ phase during recovery, and the dislocation character changed from screw component to edge component. Furthermore, the grain boundary might move by driving force of the local lattice strain around the residual γ phase in the reverse transformation.

1. Introduction

The microstructure control through optimization of constituent elements and processes has enhanced the functionality and strength of steels. Microstructures plastically deform by forging and rolling. In crystals, lattice defects such as point defects, dislocations, and stacking faults accumulate, which causes work-hardening of steel. When steel is heat-treated at high temperature, the recovery in which lattice defects including dislocations decrease occurs to reduce the free energy. In addition, the phase transformation is an important phenomenon both industrially and scientifically. Martensitic transformation is very important diffusionless transformation that controls the physical properties not only of steel but also of metals. Many researches have been performed regarding martensitic transformation in carbon steel, but it is difficult to understand the elementary processes of the recovery and phase transformation with diffusion and precipitation of carbon superposed.

For carbon free Fe-Ni alloy in which martensitic transformation also occurs, detailed reports[1, 2] on crystallographic properties and dislocation density have been made through observation using transmission electron microscopes (TEMs). These reports are very suitable for the basic study of dislocation behavior. If such dislocation substructures can be quantitatively and visually understood, not only the recovery and phase transformation behavior will be clarified, but also a new microstructure control technique may be developed that can be used for the development of a material property.

Microstructures need to be analyzed in a detailed way to understand the mechanism of development of a material property. In accordance with the sophistication of materials in terms of performance and functionality, it is necessary to improve the methods to measure and analyze fundamental structure formation and elementary processes of deformation. Neverthless, to quantify dislocation substructures that are the key to recovery and phase transformation, X-ray measurement is still an excellent method. To date, some researchers have tried to quantify changes in microstructure[3] and to estimate the dependence of accumulated strain on crystal orientation based on full width at half maximum[4] of peaks measured using X-rays. Recently, analysis of dislocation substructures has been enabled in an accurate and quantitative way using X-ray line profile analysis (XLPA)[5] based on the elastic theory.

At the same time, dislocation substructures in metal have been visually observed and evaluated using TEMs. Recently, electron channeling contrast imaging (ECCI) is attracting attention.[6, 7] In the ECCI, scanning electron microscopes (SEMs) are used to observe lattice strain caused by dislocations on the surface layer of a sample as an image showing changes in the intensities of backscattered electrons. The field of view in the ECCI observation is wider than that in the TEM observation. Some researchers have tried to observe dislocation substructures of steels and fatigue microstructures of al-

* Senior Researcher, Dr. Eng., Fundamental Metallurgy Research Lab., Advanced Technology Research Laboratories
1-8 Fuso-cho, Amagasaki, Hyogo Pref. 660-0891

loy[8–11] using this method to observe dislocation substructures of bulk samples.

In this study, in order to dynamically observe average dislocation behavior in recovery and phase transformation in Fe-Ni martensitic alloy in a quantitative way, we performed in situ X-ray diffraction measurement under high temperature. We analyzed changes in dislocation density and dislocation character at elevated temperature using the XLPA method in consideration of elastic anisotropy. In addition, using TEM and SEM-ECCI, we performed visualization of dislocation substructures together with the analysis of lattice strain distribution through the electron back scatter diffraction (EBSD) method for verification of the appropriateness of the dislocation substructures observed using the XLPA method.

2. Experimental Procedure

2.1 Chemical composition and processes

Table 1 shows the chemical composition of the alloy used in this work. The amount of Ni in Fe-Ni alloy greatly differentiates the temperature at which martensite (α') transformation begins (M_s) and the form of the α' phase.[1, 2] In this study, Fe-30 mass% Ni (with the M_s not exceeding room temperature) in which the unit size of lenticular α' crystals is relatively large was experimentally prepared. We conducted Si deoxidization to make it an extremely low-carbon alloy and analyzed the components in the alloy to check that the concentration of the impurities (elements of P, S, N, and O) had been sufficiently reduced.

Figure 1 shows a schematic view of the processes for manufacturing the samples. A 30-kg round ingot manufactured by vacuum melting was retained at 1 150°C for two hours. Then it was hot forged at 1 000°C or more to obtain a 45-mm square bar; the square bar was divided into three bars in the longitudinal direction; the three bars were retained at 1 150°C for two hours. Then they were hot rolled to 15 mm at 1 000°C or more; They were water-quenched from approximately 700°C; After that, they went through solution treatment (ST) at 1 000°C for 30 minutes and then were water-quenched. The lenticular martensite, which is formed by the combination movement of atoms, does not grow over the grain boundaries. Its size is determined by the grain size of the former austenite (γ). As the grain size of the γ after the ST was approximately 0.1 mm, coarse lenticular martensite was expected. Furthermore, a sub-zero (SZ) treatment was performed in order to obtain full martensite. In the SZ treatment, the samples were retained in liquid nitrogen (−196°C) for 30 minutes after the solution treatment.

Table 1 Chemical compositions of Fe-30 mass%Ni alloy (mass%)

C	Si	Mn	P	S	Ni	N	Al	O	Fe
0.001	0.07	0.02	<0.001	0.001	30.06	0.0008	<0.001	0.012	Bal.

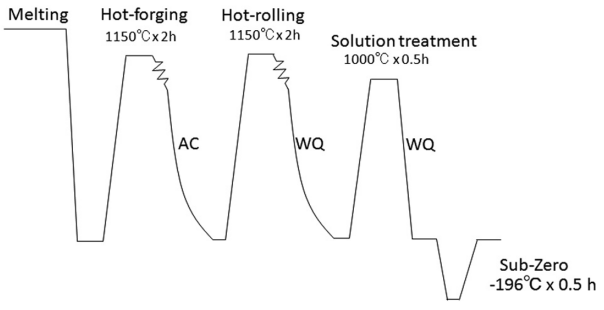

Fig. 1 Manufacturing process of Fe-30 mass%Ni alloy

Some samples were taken from these ST and SZ samples for X-ray diffraction measurement and for SEM/TEM observation. The ST sample was measured using X-ray diffraction at room temperature alone. For the samples for the X-ray diffraction, the thickness of two test pieces that were plates (15×15 mm for the measurement at room temperature and 5×5 mm for the measurement at high temperature) were reduced to 1.0 and 0.5 mm using sand paper. The measurement surfaces were polished using ultrafine sand paper and then buffed to mirror finish. The samples for SEM observation were buffed and mirror finished and then eroded using Nital. The samples for the TEM/SEM-ECCI observation in the same field of view were mechanically wet polished to 0.1 mm or less and then stamped to 3-mm diameter disks. They were electropolished by jetting perchloric acid and acetic acid electrolyte.

2.2 XRD and ECCI

In the X-ray diffraction measurement (using ULTIMA-III made by Rigaku) at room temperature, measurement was performed using the Cu wavelength (40 kV, 40 mA) in a focusing method optical system. In the two-dimensional in situ X-ray diffraction (2DXRD) measurement[12] (using Smart Lab made by Rigaku) at high temperatures, the parallel beam optical system that was not much influenced by concavity and convexity on the surface was used, because the surface of the samples would change due to thermal expansion by temperature increase and due to martensitic transformation. As the X-ray source, the Co wavelength was used for which the X-ray penetration depth was relatively large for iron alloy. Divergent X-rays (40 kV, 135 mA) emitted from the X-ray source were made pseudo parallel beam using a parabolic multilayer film mirror; were gathered to a point using an X-ray focusing mirror (CBO-*f*); and shaped to 0.5×1 mm using an incident slit. After it was irradiated to the samples in a high-temperature folder, the beam diameter was narrowed to secure angular resolution to observe changes in the Debye-Scherrer rings. A two-dimensional detector (PILATUS100K) was used for the θ-2θ scanning to measure the angle range from 40° to 130°.

A dome-type high-temperature attachment (Anton Paar DHS900) was used to cause the two dimensional X-ray scattering. The sample chamber was vacuumed using a rotary pump for two to three minutes and then N_2 gas was flowed in at 100 ml/min for few minutes. After this cycle of processes was repeated two or three times, the test pieces were measured under the N_2 atmosphere. The incident angle of the X-rays was perpendicular to the rolling direction of the test pieces in consideration of crystal orientations. The temperature profiles were 30 to 900°C. The heating rate was set to 100°C/min. The test pieces were retained at each measurement temperature for three minutes mainly every 100°C and then measured. The measurement time was approximately seven minutes. Since the CBO-*f* gathers X-rays on a sample and then X-rays scatter, the full width at half maximum (FWHM) of single crystal Si for the {220} diffraction is approximately 0.25°. This means that the dislocation density is approximately $1\times10^{13}/m^2$. The FWHM of alloy is relatively large, but when crystal grains grow under high temperature, if the FWHM is below the resolution of the optical system (i.e., $10^{12}/m^2$), the dislocation density cannot be evaluated.

For the diffraction profile of each Miller index observed, diffraction from the $K\alpha_1$ and $K\alpha_2$ rays was separated by fitting by the *pseudo*-Voigt function that was indicated as a simple sum of the Gauss function and the Lorentz function. In addition, the α' and γ phases

were separated and the FWHM of the $K\alpha_1$ ray of each phase was extracted. The measured diffraction intensity is convolution of the instrumental function and the intrinsic profile function of material. To obtain the intrinsic profile function, the instrumental function needs to be deconvolved from the experimental data.[13] This correction can be made by means of relatively simple mathematics from the FWHM of the material used in the experiment and standard sample using the *pseudo*-Voigt function. As the standard sample, LaB_6 (NIST SRM 660b) was used because its crystallinity was good and the grain diameter was fine (15 μm or less) and uniform. It is also best suited to correcting FWHM. As a lattice constant and phase fraction analysis, the Rietveld method was applied. The method optimizes crystal structures through optical correction and a strict diffracted intensity formula.[14]

The TEM observation (using Titan made by FEI) was carried out in the scanning transmission electron microscope (STEM) mode at 300 kV. In the SEM-ECCI (using Versa3D made by FEI), the initial SZ texture was observed using an insertion-type concentric-back-scattered electron (CBS) detector at the acceleration voltage of 5 kV and the working distance (WD) of 9.0 mm. In the SEM-ECCI (using Scios made by FEI) for observation in the same field of view as STEM images, the CBS detector was used for observation at the acceleration voltage of 20 kV and the WD of 5.5 mm. As the dislocation contrast in the ECCI is caused by deviation of the Broch wave from the Bragg condition, the dislocation contrast is susceptible to crystal orientations.[9, 10] A few degrees of inclination of a sample cause the contrast to vary.[15] Therefore, the dislocation contrast in the ECCI was compared to that of the STEM image for evaluation.

Furthermore, the locations where the α' and γ phases existed were identified through crystal orientation distribution analysis in the SEM-EBSD; and grain reference orientation deviation (GROD) analysis was performed using an orientation imaging microscopy analyzer made by TSL. GROD is an orientation difference between the orientation of the measurement point that is determined as the reference point in a grain and the orientation of another measurement point in the grain, indicating the lattice strain distribution in the grain. In other words, GROD contains information on local dislocation accumulation and distribution. We compared it to the macroscopic average value of the X-ray dislocation density.

2.3 XLPA analysis

The introduction of dislocations into plastically deformed metallographic structures causes lattice strain and low-angle grain boundaries and cell structures develop in accordance with dislocation arrangement. When such dislocations and domain structures as a result of such dislocations are captured as X-ray diffraction patterns, the diffraction peaks show the characteristic spread and shape of the line profile depending on the diffraction index. To separate information on the dislocations and stacking faults and convert the information into numbers by the XLPA method, various analysis methods such as the Williamson-Hall method and the Warren-Averbach method were formulated in the 1950s.[16, 17]

Recently, quantitative analysis of dislocation density and character from lattice strain based on the elasticity theory has been theoretically developed mainly in Europe and the U.S. In particular, the theory proposed by Ungár, et al.[5] explains the relationship between dislocations and line profiles most successfully. The theory by Ungár, et al. analyzes line profiles based on the strain occurring in an anisotropic way to crystal orientations and magnitude of strain fields that dislocations have. Specifically, the Burger's vector of dislocations causes strong lattice strain in a specific crystal orientation depending on the crystal system. The XLPA method using the *modified* Williamson-Hall method and *modified* Warren-Averbach method based on the elastic anisotropy has made it possible to quantitatively evaluate the dislocation density of various materials, magnitude of dislocation strain fields, and fractions of edge and screw dislocation components.

The *modified* Williams-Hall formula is expressed as equation (1) with ΔK^D (the term for strain) as follows,

$$\Delta K = 0.9/D + (\pi M^2 b^2/2)^{1/2} \cdot \rho^{1/2} K\overline{C}^{1/2} + O(K^2\overline{C}) \quad (1)$$

where M is a constant depending on the effective outer cut-off radius of dislocations and O indicates non-interpreted higher order terms, b is the Burger's vector, ρ is the dislocation density, and $\overline{C}$ is the average contrast factor. The *modified* Warren-Averbach formula where R_e is the effective outer cut off radius of dislocations is expressed as equation (2).

$$\ln A(L) = \ln A^s(L) - \rho \cdot \pi b^2/2 \cdot L^2 \cdot \ln(R_e/L) \cdot (K^2\overline{C}) + Q(K^4\overline{C}^2) \quad (2)$$

$\overline{C}$ included in equations (1) and (2) is calculated from elastic compliance and gives elastic anisotropy to each Miller index. Therefore, in in situ X-ray diffraction measurement at high temperatures, the dependence of the elastic constant on temperature must be considered using the XLPA method.

Here, $\overline{C}$ at every mirror index can be written as

$$\overline{C}_i = \overline{C}_{h00}\,(1 - qH_i^2)$$

q is related to dislocation character such as edge or screw. H depends on the mirror index (h, k, l) in the cubic crystal system as the following function.

$$H_i^2 = (h_i^2k_i^2 + h_i^2l_i^2 + k_i^2l_i^2)/(h_i^2 + k_i^2 + l_i^2)$$

$\overline{C}_{hoo}$ 0.285 in the case of pure iron. Then, q is 1.2 in 100% edge dislocation and 2.8 in 100% screw dislocation. The fraction of screw dislocation is calculated by the ratio of q.

3. Results and Discussion

3.1 Microstructure observation

Figure 2(a) shows an SEM-ECCI image of the SZ material. On this ECCI image, concavo-convex information on the surface is superposed, showing large lenticular martensite microstructure that has grown like bamboo leaves and wavy small martensite crystals (microstructure in the shape of lightning) formed in a chain reaction. The middle of the lenticular martensite plate called mid-rib is the region in which high density of transformation twins exists. It is reported that its average width is approximately 190 nm.[18] The ECCI image of this SZ material in Fig. 2(b) clearly shows high-density (112) twin crystals of the mid-rib in a bright linear contrast. The average core width is approximately 200 nm. Lenticular martensite dislocation substructures were confirmed as expected.

3.2 Two-dimensional in situ X-ray diffraction

Figure 3 shows excerpted in situ 2DXRD patterns that are characteristic of SZ materials observed in the process of elevated temperature. The horizontal axis indicates the diffraction angle (2θ) and β is the direction of the ring. At room temperature (30°C), relatively ring-like diffraction patterns of the α' phase and spot-like diffraction patterns of the residual γ phase indicated by arrows in the figure are observed in the β direction. This means that this SZ material has not reached full martensitic transformation. As the temperature continuously increases, changes can be seen at 400°C. Then the diffraction spots of the residual γ phase become brighter; and the spots spread to the β direction, combining with each other. It has been reported that in the Fe-Ni alloy, when the α' phase transforms to the γ phase,

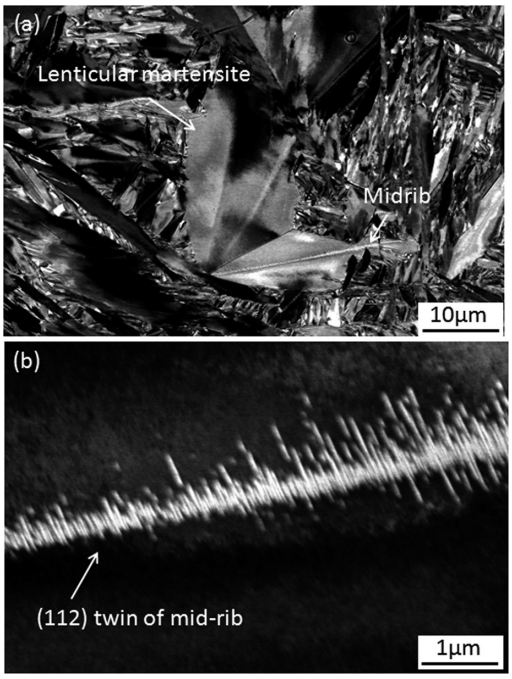

Fig. 2 Microstructures of lenticular martensite (a) and ECCI of mid-rib (b) in the sub-zero treated Fe-30mass%Ni alloys

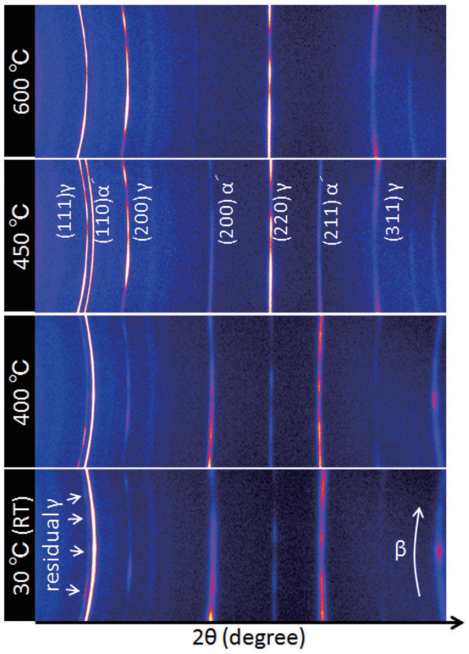

Fig. 3 In situ 2DXRD patterns of Fe-30mass%Ni alloy at any temperature

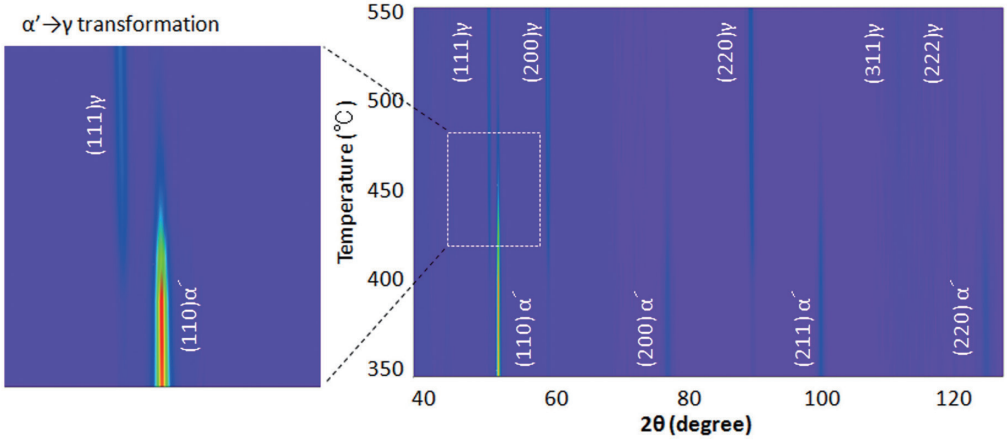

Fig. 4 Temperature dependency of X-ray diffraction intensity of Fe-30mass%Ni alloy

the boundary between the γ and α' phases cannot migrate and the nucleation of the new γ phase occurs in α' crystals or on the boundary between the γ and α' phases.[19] Based on the behavior in this reciprocal space, when the residual γ phase has spread widely in the initial microstructure, the γ phase may be preferentially allowed to grow with such residual γ phase as a core. When the diffraction rings change to show the clear γ phase at 600°C, most of the α' phase disappears and only the γ phase is observed.

The measured two-dimensional patterns were integrated in the β direction and line profiles (2θ-I) were made to obtain diffracted intensity (I). **Figure 4** shows this change of intensity (I) at elevated temperatures. The α' phase mainly exists at low temperatures. Reverse transformation (from the α' phase to the γ phase) is observed at around 400°C. A little shift of the diffraction peak toward a lower angle due to thermal expansion is also observed. To extract dynamic dislocation recovery and phase transformation behavior in this process of elevated temperature, the XLPA method was applied to the four α' phase diffraction profiles for {110}, {200}, {211}, and {220} and the four γ phase diffraction profiles for {111}, {200}, {220}, and {311} at each temperature.

3.3 Thermal expansion and phase fraction

Figure 5 shows the lattice constant and temperature change. As described above, the diffraction angle is displaced due to thermal expansion, which causes phase transformation. While Fe-30mass%Ni alloy creates no special ordered lattices, the α' phase is a cubic crystal system as is the case with pure iron.[20] Temperature rise causes the Bain deformation from the bcc-α' phase to the fcc-γ phase without diffusion. Changes in crystal lattices significantly cause the lattice constant to vary. In the α' phase, the lattice constant changes almost linearly. However, the lattice constant change of the γ phase shows a convex shape at an early stage of the transformation and then changes linearly. In the Fe-Cr alloy, rapid expansion has

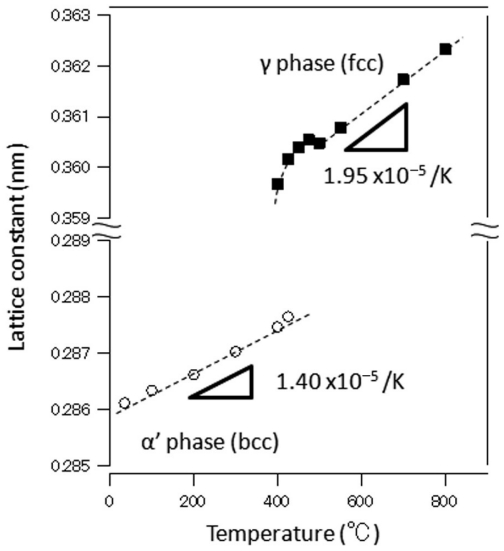

Fig. 5 Displacement of the lattice constant of α' and γ phases at elevated temperature

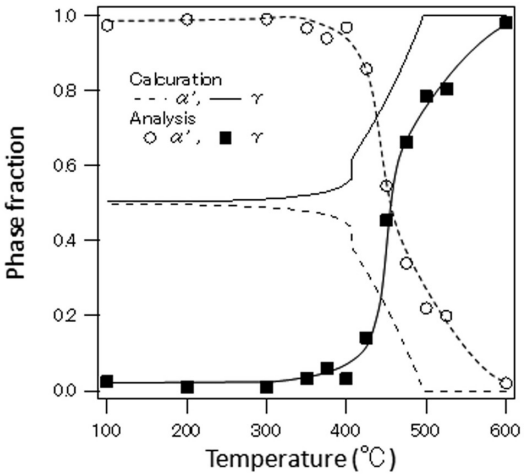

Fig. 6 Temperature dependency of measured and calculated fraction of α' and γ phases

Table 2 Dislocation density of ST and SZ alloys at room temperature

Thermal treatment	ST		SZ	
Phase	α'	γ	α'	γ
Dislocation density (/m^2)	6.8×10^{14}	2.2×10^{13}	6.2×10^{14}	8.0×10^{14}
Rate of screw component (%)	0.92	0.55	0.92	0.59

been observed due to martensitic transformation at an early stage of the transformation from the α phase to the γ phase in a measurement using a thermal expansion meter. The following contraction due to diffusion transformation has also been reported.[21]

Martensitic transformation in Fe-30 mass% Ni alloy is a rapid Umklapp transformation in which the propagation velocity is approximately 10^3 m/s.[22] Strain caused by transformation from the α' phase to the γ phase accompanied by uniform strain is considered to influence the occurrence of relatively sharp thermal expansion of the γ phase at the time of reverse transformation. After linear approximation, the linear expansion coefficient is 1.95×10^{-5}/K for the γ phase and 1.40×10^{-5}/K for the α' phase. In a report regarding Fe-30 mass% Ni alloy,[23] it is 2.30×10^{-5}/K for the γ phase and 1.03×10^{-5}/K for the α' phase, almost equal to the measured values in this study.

Next, regarding phase fraction, thermal equilibrium calculation (Termocalc ver. S, TTFE database) was compared to the analysis results. **Figure 6** shows the comparison results. In the thermal equilibrium calculation, the fractions of the α' and γ phases are 50% respectively at room temperature. As the temperature increases, the γ phase becomes 100% at 500°C. On the other hand, while the residual γ phase of approximately 2% exists in the SZ material, the α' phase accounts for approximately 98% at room temperature. The γ phase increases in the reverse transformation and the state transits to one of thermal equilibrium. The temperature at which the transformation starts (A_s) is approximately 400°C, which is almost equal to the temperature obtained by the thermal equilibrium calculation. The temperature at which the transformation finishes (A_f) is approximately 600°C, higher than the thermal equilibrium temperature.

3.4 Dislocation density and dislocation character

First, in order to analyze phase fractions on a few percent level, the ST and SZ materials were measured using X-ray diffraction at room temperature. **Table 2** shows the XLPA results. The dislocation density of the matrix (γ phase) of the ST material is 2.2×10^{13}/m^2. The lattice strain was relaxed (recovery) overall. The thermal equilibrium dislocation density after the recovery reached the limit of X-ray measurement or more. The dislocation density of the α' phase that accounts for approximately 2% of the ST material is large at 6.8×10^{14}/m^2. This dislocation density of the α' phase may be martensite[24] on the surface produced by preparation of the test piece.

Secondly, the dislocation density of the α' phase of the SZ material after the martensitic transformation is 6.2×10^{14}/m^2. This is equivalent to the elastic strain energy of 7.2 J/mol. While the driving force of martensitic transformation is large at approximately 10^3 J/mol, the elastic strain energy after the transformation is almost equal to that of lath martensite of 9Cr steel.[25] In addition, the dislocation density of the residual γ phase, which was approximately 2% of the SZ material shown in Fig. 3, is 8.0×10^{14}/m^2, overall according with the dislocation density of Fe-30 mass% Ni alloy measured using TEM[2] that was 0.6 to 1×10^{15}/m^2 for the α' phase and 0.4 to 0.6 $\times10^{15}$/m^2 for the γ phase. In the α' phase of the SZ material after the transformation, high-density dislocation substructures constituted mainly by screw dislocations were formed. In addition, the dislocation density of the residual γ phase of the SZ material is one digit larger than that of the γ phase of the ST material in which the strain was mitigated. This is a result of plastic deformation of the γ phase due to the relaxed strain associated with the martensitic transformation.

Regarding dislocation characteristics, approximately 92% is screw components for the α' phase of both ST and SZ materials. In contrast, for the γ phase, edge components account for approximately 40%, showing distinctive differences. The Peierls potential is different between screw dislocations and edge dislocations. An edge dislocation is in a planar structure[26] in which only one slip plane (111) has atomic displacement distribution and the dislocation migration readily migrates by relatively small Peierls stress. On the other hand, a screw dislocation is in a non-planar structure[27] in which, if slip on the $(01\bar{1})$ plane is assumed, there is also atomic displacement distribution on the $(10\bar{1})$ and $(1\bar{1}0)$ planes with which the (011) plane shares the slip direction [111] (and these two planes are equivalent to the (011) plane) due to the influence of the elastic

field. Thus, there is a large mobility barrier for a screw dislocation. This causes the Peierls stress to be large for screw dislocations, and therefore it is expected that an increase in the fraction of screw dislocations allows improvement of the strength with the same dislocation density.

Thirdly, **Fig. 7** shows the XLPA results of the high-temperature in situ X-ray diffraction. In the in situ measurement, the diffraction intensity of the residual γ phase of the SZ material was small. The fraction of the γ phase started increasing at 400°C (phase transformation temperature) and analyzable diffraction intensity was obtained. The diffraction peak shifted as the temperature increased. As the thermal vibration parameter (B) became larger, the diffraction intensity decreased on the higher angle side due to influence of the Debye-Waller factor.[28] The FWHM was strictly determined using the FWHM parameter in the X-ray diffraction intensity formula and thereby it did not rely on temperature. Therefore, in the XLPA of X-ray diffraction at high temperature, the diffraction angles and the elastic compliance as described above must be corrected.

Figure 7(a) shows changes in the dislocation density in the process of the temperature increasing. The dislocation density significantly decreased at 400°C and the α' phase inversely transformed to the γ phase reversibly during the recovery. In this reverse transformation, high-density dislocations of approximately 2×10^{14}/m^2 that existed in the α' phase were taken over when the α' phase transformed to the γ phase. Then, after the dislocation density change of the γ phase was retarded, which was possibly due to the influence of transformation strain, the dislocation recovery started. The dislocation density decreased to 1.2×10^{13}/m^2 that is equal to that of the γ phase of the ST material. As with the case of a proposed model in which in Fe-Ni-C alloy and Cu-Zn alloy, twin dislocations are discharged to the matrix from the α' crystals during phase boundary migration in reverse transformation that has also been verified in experiments,[29, 30] it is highly likely that the γ phase takes over the dislocation density from the α' phase in a similar mechanism.

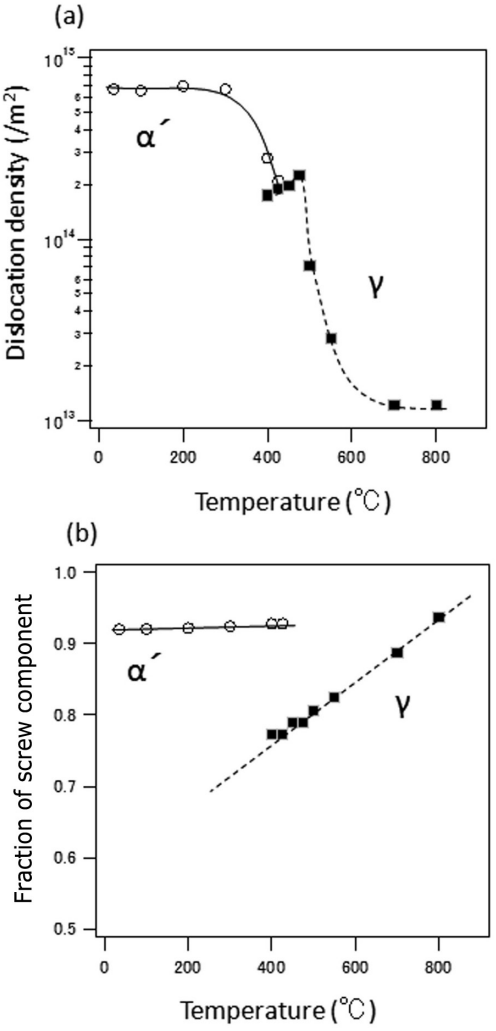

Fig. 7 Dynamic change of dislocation density (a) and character (b) at elevated temperature

However, although the dislocation density is taken over in the reverse transformation, the dislocation character is completely different. As shown in Fig. 7(b), during the elementary process, the dislocation characteristics for the α' phase did not change much up to 400°C and screw components accounted for approximately 90%. In the γ phase during the reverse transformation, relatively many edge components were seen and the screw components increased to approximately 90% from approximately 75% as the temperature increased. We consider that this was attributable to the dislocation character of the SZ material shown in Table 2. Specifically, the rate of the edge components in the residual γ phase was approximately 55% at an early stage. As the temperature increases, such components continuously decrease and then recover. This is possibly due to the large mobility of dislocations due to the Peierls potential[25] of edge dislocations that is one digit smaller than that of screw dislocations. In addition, as the dislocation density decreased, the main rate-determining processes of the recovery are the incorporation and disappearance of dipoles due to the climbing motion of edge dislocations.

3.5 Observation in the same field of view by STEM and ECCI

Next, in order to identify dislocation substructures, the sample for TEM observation was studied through ECCI and then the same field of view was observed using a TEM. **Figure 8**(a) shows an STEM image of the center of a lenticular martensite crystal and 8(b) shows an ECC image of the same. According to a detailed TEM observation of the Fe-Ni lenticular martensite alloy, the mid-rib at the center was high-density (112) twin crystals. The areas around the mid-rib were constituted by (112) twin crystals and screw dislocations, while the areas in the vicinity of the interface of the γ phase consisted of microstructures in which dislocations entangled with each other in a complicated way.[18]

In the STEM image and ECC image in Fig. 8, there is the (112) twining plane tilted by approximately 50° from the mid-rib at the center, and contrast possibly constituted by screw dislocations can be observed as well around the mid-rib. The dark contrast domain on the right side in the ECC image satisfies the channeling conditions. Comparing this to the STEM image, the bright linear contrast is considered to be the twin plane and dislocations. These high-density screw dislocations possibly correspond to the dislocation density and character of the α' phase of the SZ material shown in Table 2.

In the STEM and SEM observations, as the inclinations of the sample do not exactly match up, the images cannot be simply compared. To evaluate defects observed through ECCI, noise of the STEM and ECC images was removed by image analysis, sections at which the brightness sharply changed in the images were extracted (binarization), and the ratio of the area of the twin plane and the dislocation line contrast to the total number of pixels in the observation

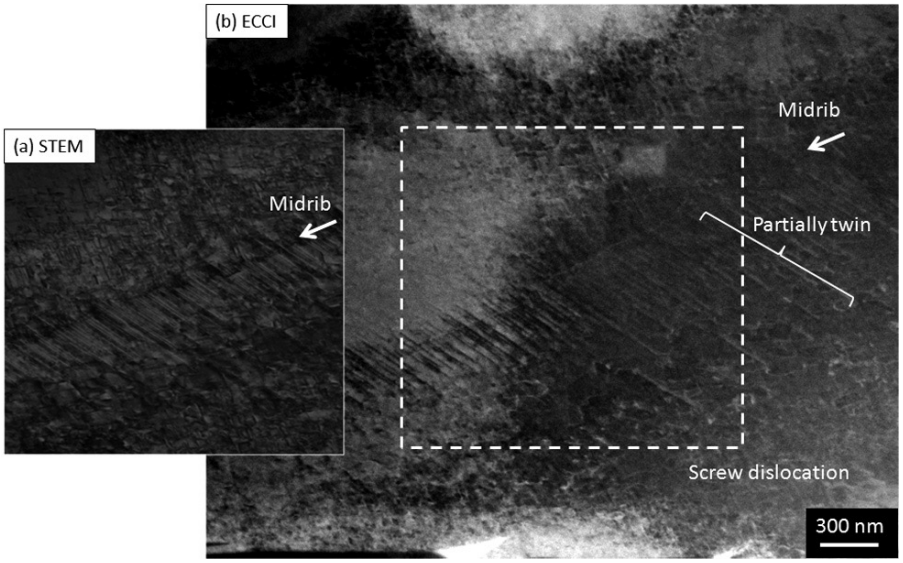

Fig. 8 STEM image (a) and ECCI (b) of same lenticular martensite in the sub-zero treated Fe-30mass%Ni alloy

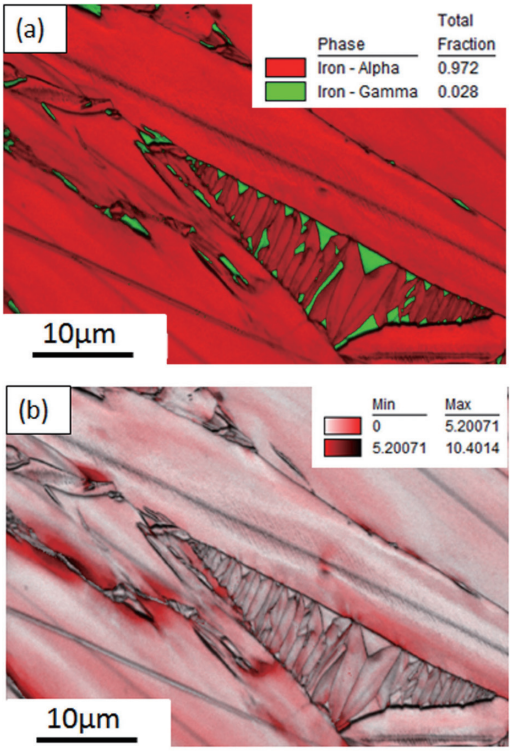

Fig. 9 Phase map (a) and GROD map (b) of the sub-zero treated Fe-30mass%Ni alloy

field of view was calculated. When it is assumed that the STEM image in Fig. 8(a) shows the information on the screw dislocations and twin plane and it is used as the reference (18.5), approximately 70% (13.8/18.5) of material defects may have been detected in the ECC image in Fig. 8(b). In addition, regarding the (112) twining plane of the mid-rib of the alloy and the surrounding screw dislocation contrast, the ECC image well accords with the STEM image visually, so we think that plane defects can be observed in TEM observation.

3.6 Residual γ phase and distribution of lattice strain

Lastly, the location where the residual γ phase of the SZ material existed was identified using a phase map through EBSD and the lattice strain distribution was analyzed through GROD. As shown in **Fig. 9**(a), the residual γ phase was distributed finely mainly at α' phase interfaces. At a chain of small α' crystal interfaces, triangle shapes that are possibly the habit plane of {111} were observed. The fraction of the residual γ phase was approximately 2% as a result of an analysis using the X-ray Rietveld method; and it is also approximately 3% in the phase map, well according with the result of the X-ray Rietveld analysis, although this was a result for only a single field of view. Next, as shown in Fig. 9(b), in the lattice strain distribution analyzed through GROD, large sections (dark red areas in the figure) locally exist around the residual γ phase at large lenticular martensite crystal interfaces, but mostly the α' and γ phases prevail, showing uniform lattice strain overall. As shown in Table 2, the average X-ray dislocation density of the α' and γ phases of the SZ material is at the same level at approximately 6 to $8\times10^{14}/m^2$, so they match qualitatively. In addition, the areas with large local lattice strain indicate the existence of plastic strain accumulated in the α' phase around the residual γ phase. In the phase transformation at elevated temperature, such plastic strain may work as the driving force of grain boundary migration and may encourage the growth of the residual γ phase. This is also considered to apply to the growth of crystal grains with the residual γ phase as their core observed in Fig. 3.

4. Conclusion

We observed the dislocation substructures of Fe-30mass%Ni lenticular martensite by in situ 2DXRD and STEM/ECCI along with EBSD. The dislocation density of the α' and γ phases was analyzed using the XLPA method. We found that during the phase transformation in the process of recovery from the α' phase to the γ phase, the dislocation density is taken over, and the prevailing dislocation character changes from screw components to edge components. In addition, phase transformation may be caused by grain boundary migration with local lattice strain around the residual γ phase as the driving force. Furthermore, consideration while comparing an ECC

image to dislocation substructures in a STEM image becomes possible, allowing defects to be observed in TEM observation. We expect that the method in this study can make a significant contribution to the analysis of dislocation substructures of steels.

Acknowledgments

We would like to express our appreciation to Ms. Rina Takizawa who participated in our research as an intern at our company from the Interdisciplinary Graduate School of Engineering Sciences, Kyushu University, for her help in undertaking this study. We also express our gratitude to Professor Minoru Nishida and Associate Professor Masaru Itakura at the Faculty of Engineering Sciences, Kyushu University, for their advice and instructions on TEM and SEM observation, as well as to Professor Hideharu Nakashima, Associate Professor Masatoshi Mitsuhara, and Research Fellow Shigeto Yamasaki, for their support when they kindly allowed us to use the equipment at the university.

References

1) Reed, R. P.: Acta Mat. 15, 1287 (1967)
2) Shibata, A. et al.: Mater. Sci. Eng. A438–440, 241 (2006)
3) Decker, B.F. et al.: Trans AIME. 188, 887 (1950)
4) Shiraiwa, T. et al.: Journal of the Japan Institute of Metals and Materials. 35, 20 (1971)
5) Ungár, T. et al.: Appl. Phys. Lett. 69, 3173 (1996)
6) The Surface Science Society of Japan: Scanning Electron Microscopes for Nanotechnology. 4th Impression, Tokyo, Maruzen Publishing, 2009
7) Trager-Cowan, C. et al.: Phys. Rev. B. 75, 085301-8 (2007)
8) Kaneko, Y. et al.: Mater. Sci. Eng. A 400–401, 413 (2005)
9) Hashimoto, S. et al.: Function & Materials. 30 (7), 69 (2010)
10) Sugiyama, M. et al.: Bulletin of the Japanese Society of Microscopy. 48 (3), 216 (2013)
11) Zaefferer, S. et al.: Acta Mater. 75, 20 (2014)
12) Yonemura, M.: In-situ Measurement/In-situ Observation Actual Cases. 1st Ed., Tokyo, Johokiko Co., Ltd. 2013, p. 98
13) Klug, H.P. et al.: X-ray Diffraction Procedure. 2nd Ed. John Wiley & Sons, 1902, p. 291
14) Rietveld, H.M.: J. Appl. Crystallogr. 2, 65 (1969)
15) JEOL Application Data Sheet. SM-A-004-00, JEOL Ltd. Tokyo
16) Williamson, G.K. et al.: Acta Metal. 1, 22 (1953)
17) Warren, B.E. et al.: J. Appl. Phys. 21, 595 (1950)
18) Shibata, A. et al.: Acta Mat. 57, 483 (2009)
19) Kessler, H. et al.: Arch. Eisenhütten-Wers. 38, 589 (1982)
20) Nishiyama Z.: Martensitic Transformation. 1st Ed. Tokyo, Maruzen Publishing, 1971, p. 16
21) Lacoude, M. et al.: Compt. Rend. Group 7. 259, 1858 (1964)
22) Honma, T: J. Japan Inst. Met. Mater. 21, 126 (1957)
23) Oomi, G. et al.: J. Phy. Soc. Jpn. 50, 2924 (1981)
24) Okada, M. et al.: Techn. Rep. Osaka Univ. 5, 169 (1955)
25) Kunieda, T. et al.: ISIJ Int. 45, 1907 (2005)
26) Vitek, V.: Philos. Mag. 84, 415 (2004)
27) Lung, C.: J. Mater. Sci. Technol. 11, 133 (1995)
28) Nakai. I. et al.: Practical X-ray Structure Analysis. 1st Ed. Tokyo, The Japan Society for Analytical Chemistry, 2002, p. 97
29) Kajiwara, S. et al.: Phil. Mag. A. 48, 509 (1983)
30) Kajiwara, S. et al.: Acta Metall. 30, 589 (1982)

Mitsuharu YONEMURA
Senior Researcher, Dr. Eng.
Fundamental Metallurgy Research Lab.
Advanced Technology Research Laboratories
1-8 Fuso-cho, Amagasaki, Hyogo Pref. 660-0891

Tomohiro NISHIURA
Researcher, Dr. Eng.
Fundamental Metallurgy Research Lab.
Advanced Technology Research Laboratories